

## ANNEALING TIME EFFECT ON NANOSTRUCTURED n-ZnO/p-Si HETEROJUNCTION PHOTODETECTOR PERFORMANCE

NADIR. F. HABUBI\*, RAID. A. ISMAIL<sup>†,‡</sup>, WALID K. HAMOUDI<sup>†</sup>  
and HASSAM. R. ABID\*

\*Department of Physics, College of Education  
University of Al-Mustansiriyah, Baghdad, Iraq

<sup>†</sup>Department of Applied Sciences  
University of Technology, Baghdad, Iraq  
<sup>‡</sup>raidismail@yahoo.com

Received 16 December 2014

Revised 17 January 2015

Accepted 26 January 2015

Published 25 February 2015

In this work, n-ZnO/p-Si heterojunction photodetectors were prepared by drop casting of ZnO nanoparticles (NPs) on single crystal p-type silicon substrates, followed by (15–60) min; step-annealing at 600°C. Structural, electrical, and optical properties of the ZnO NPs films deposited on quartz substrates were studied as a function of annealing time. X-ray diffraction studies showed a polycrystalline, hexagonal wurtzite nanostructured ZnO with preferential orientation along the (100) plane. Atomic force microscopy measurements showed an average ZnO grain size within the range of 75.9 nm–99.9 nm with a corresponding root mean square (RMS) surface roughness between 0.51 nm–2.16 nm. Dark and under illumination current–voltage ( $I-V$ ) characteristics of the n-ZnO/p-Si heterojunction photodetectors showed an improving rectification ratio and a decreasing saturation current at longer annealing time with an ideality factor of 3 obtained at 60 min annealing time. Capacitance–voltage ( $C-V$ ) characteristics of heterojunctions were investigated in order to estimate the built-in-voltage and junction type. The photodetectors, fabricated at optimum annealing time, exhibited good linearity characteristics. Maximum sensitivity was obtained when ZnO/Si heterojunctions were annealed at 60 min. Two peaks of response, located at 650 nm and 850 nm, were observed with sensitivities of 0.12–0.19 A/W and 0.18–0.39 A/W, respectively. Detectivity of the photodetectors as function of annealing time was estimated.

*Keywords:* ZnO nanoparticles; photodetectors; drop casting; annealing.

PACS Nos.: 73.50.Gr, 73.50.Pz, 78.67.BF, 68.55.ag, 68.37.Ps, 68.47.Fg

### 1. Introduction

Zinc oxide (ZnO) is a very versatile and promising material,<sup>1–3</sup> having unique piezoelectric and transparent conducting properties among semiconducting oxides. Its high electrical conductivity and optical

transmittance in the visible region make it an ideal candidate as transparent conducting electrodes in flat panel displays and window layers of solar cells.<sup>4–6</sup> The wide band gap (3.37 eV) and exciton binding energy (60 meV) facilitate its high potential applications; as

<sup>‡</sup>Corresponding author.

laser diodes, solar cells, gas sensors, optoelectronic devices, UV detectors, etc. In addition, its wide band gap can enable high temperature and power operations.<sup>7–9</sup> The synthesis and properties of various ZnO nanorods, nanowires, nanotubes, quantum wells and nanoparticles (NPs), have been reported.<sup>10–14</sup> Among these, the NP nanostructure could be of fundamental importance as a three-dimensional confined system, bridging the gap between bulk materials and molecular compounds. ZnO nanostructures exhibit a strong green photoluminescence which helps fabricating high performance photodetectors. In addition, ZnO nano-materials have been studied to reduce dark noise, to increase absorption efficiency and to explore the potential for large area and lower cost devices.<sup>15</sup> Metal organic chemical vapor deposition (MOCVD), spray pyrolysis, ion beam assisted deposition, laser-ablation, sputter deposition, template assisted growth and chemical vapor deposition are some of the techniques employed to synthesis ZnO NPs.<sup>16–23</sup> Silicon based heterojunctions photodetectors are used widely due to their superior high responsivity, fast response time, good linearity characteristics, low dark current and long wavelength detection.<sup>24,25</sup> In the current work, we present the effect of annealing time on the characteristics of ZnO/Si heterojunction photodetectors prepared by drop casting of ZnO NPs films on silicon substrates.

## 2. Experimental Details

High purity ZnO was ground by ball milling equipment in order to obtain nanoscale ZnO particles. A 60 ml of double distilled water (DDW) was mixed with 0.2 M of ZnO NPs using a magnetic stirrer for 20 min. The synthesized ZnO NPs were drop-casted on both: quartz and p-type (111) Si substrates. The  $5 \Omega \cdot \text{cm}$  resistivity silicon substrates were first cleaned with RCA standard method and then treated with HF to remove the native oxide. After drop casting the ZnO NPs on quartz and silicon substrates were dried at  $80^\circ\text{C}$  then annealed at a constant temperature of  $600^\circ\text{C}$  in air for different time intervals (15, 30, 45 and 60) min using tube furnace. The morphology of the grown ZnO NPs was investigated with the aid of an atomic force microscope AFM (SPM AA3000 Angstrom). X-ray diffractometer (Rigaku Ruzhr,  $\text{CuK}\alpha$  radiation) was used to investigate the structure of ZnO NPs drop casted on

silicon. The 300 nm thickness of the ZnO films, deposited on quartz substrates, were measured with the aid of ellipsometer and their optical properties were examined using a SHIMADZU UV-1650 PC, (200–900) nm spectrophotometer. Besides, the ZnO NPs electrical properties were tested by employing Hall measurements. Aluminum films were deposited on both sides, the ZnO film and the Si through a special mask to establish ohmic contacts. Dark and illuminated  $I-V$  characteristics were investigated.  $C-V$  measurements were carried out using LCZ meter at frequency of 100 kHz. Finally, (400–900 nm) monochromator was utilized to measure the spectral responsivity of the photodetectors using a calibrated silicon power meter.

## 3. Results and Discussion

Figure 1 shows XRD patterns of a ZnO thin film annealed at  $600^\circ\text{C}$  for different times. It reveals a

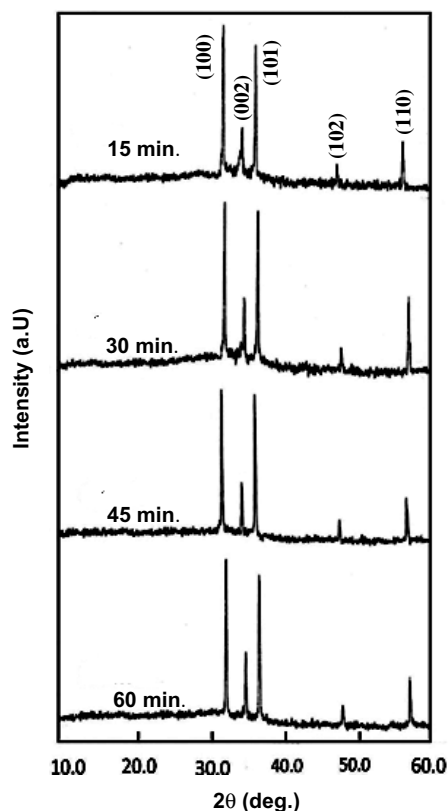


Fig. 1. XRD patterns of ZnO nanoparticles drop casted on silicon annealed at different times: (a) 15 min, (b) 30 min, (c) 45 min and (d) 60 min.

Table 1. Lattice parameters of ZnO NPs annealed at different times.

$t_A$	(100) plane			(002) plane			(101) plane		
	$2\theta$	$I/I_o$	d (nm)	$2\theta$	$I/I_o$	d (nm)	$2\theta$	$I/I_o$	d (nm)
ASTM		71	0.2816		56	0.2602		100	0.2476
15 min	31.66	100	0.2822	34.3	45	0.2611	36.14	97	0.2482
30 min	31.71	100	0.2818	34.3	50	0.2611	36.16	92	0.2481
45 min	31.73	100	0.2816	34.36	46	0.2606	36.20	86	0.2478
60 min	31.75	100	0.2814	34.41	50	0.2603	36.23	94	0.2476

prominent peak (100) and other orientations. Three distinct peaks indexed to (100), (002) and (101) diffraction planes can be recognized (JCPDS#1314-13-2) at  $2\theta = 31^\circ$ ,  $34.2^\circ$  and  $36^\circ$  respectively. No other incomplete phases are observed in Fig. 1. The synthesized films are polycrystalline in nature revealing a wurtzite ZnO hexagonal structure.<sup>26</sup> The prepared pure ZnO thin film has a (100) preferred orientation with (101) and (002) orientations, observed comparatively with lesser intensities. The long time annealing has permitted a slight increase in the diffraction intensity due to the enhanced films' quality in agreement with reported results.<sup>23</sup> Table 1 shows the main XRD parameters of ZnO NPs annealed at different times. Figure 2 presents the effect of annealing time on optical transmittance spectra of the ZnO NPs films. Films annealed for 60 min shows maximum average optical transmittance due to the improved structural stoichiometry and the reduced trapping centers. The latter usually shift the absorption edge

to higher energy. The optical band gap of ZnO NPs films was calculated by extrapolating the straight line of  $(\alpha h\nu)^2$  versus photon energy ( $h\nu$ ) plot to  $h\nu$  axis. Table 2 lists the values of the optical band gap as a function of annealing time. The band gap decreases as annealing time increases (absorption edge shifts towards long wavelengths). This may be due to the increasing ZnO particles' size after annealing for longer time (grain growth). The estimated band gap values are wider than that of the bulk ZnO because of the quantum size effect. Figure 3 shows 2D and 3D AFM images of ZnO NPs annealed at different times. They indicate the formation of spherical-like shape compact NPs; distributed with individual columnar grains extending upwards. The root mean square (RMS) surface roughness and average grain sizes are listed in Table 3, indicating an increasing surface roughness and average grain size with annealing time. Longer annealing time improves grain growth and produces high porosity films. Hall measurements confirm the n-type nature of all annealed ZnO film (due to excess the oxygen vacancies), indicating the formation of anisotype ZnO/Si (n-p) heterojunctions. Figure 4 shows the variation of mobility and carrier concentration of ZnO NPs films with annealing time. The carrier mobility ( $\mu_n$ ) was estimated from Hall measurement using the following equation:

$$\mu_n = -\sigma_n R_H, \quad (1)$$

Table 2. Dependence of optical energy gap on annealing time.

$t_A$ (min)	Optical energy gap (eV)
15	3.54
30	3.46
45	3.4
60	3.3

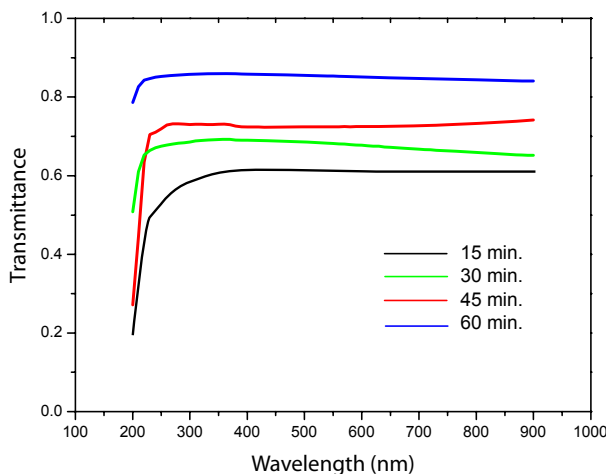


Fig. 2. Transmittance versus wavelength plot of annealed ZnO NPs.

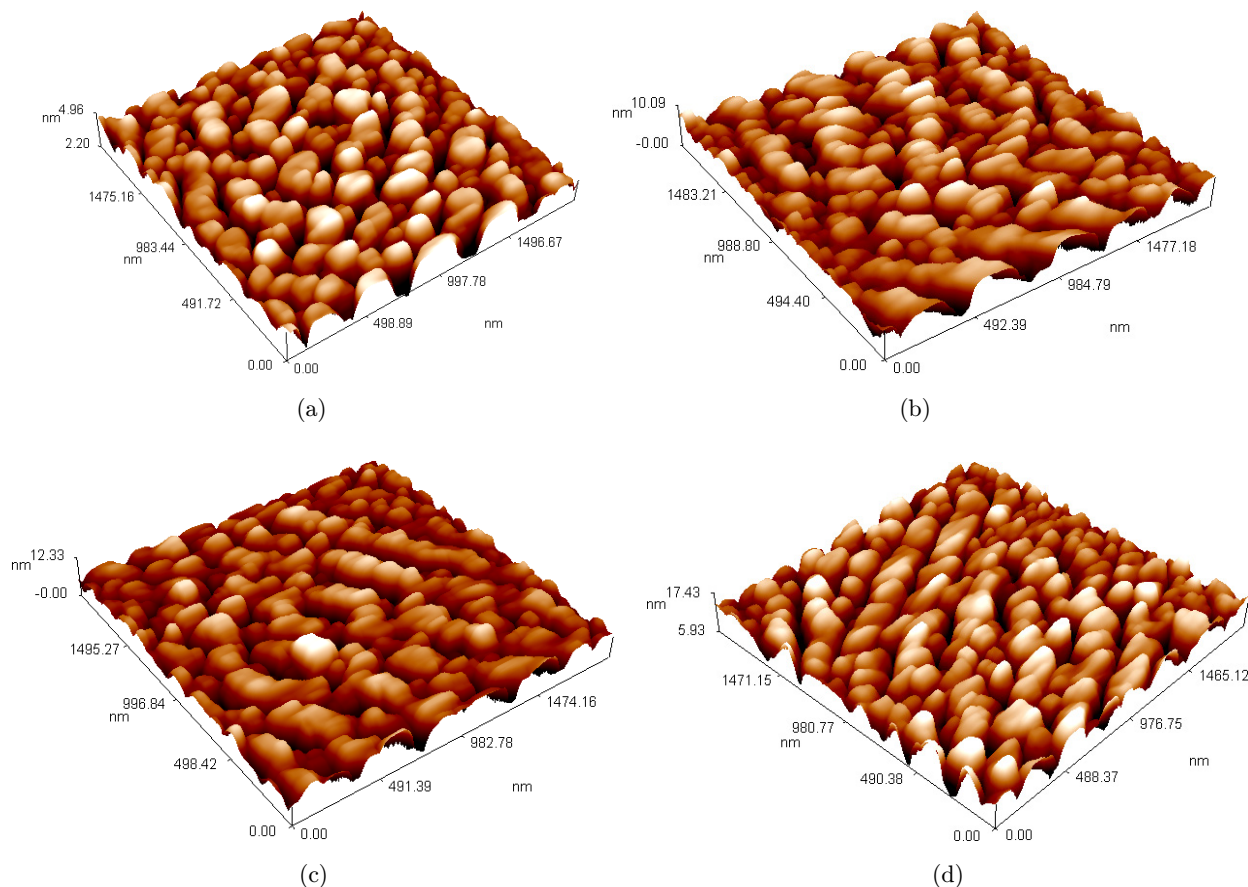


Fig. 3. 2D and 3D AFM images of ZnO nanoparticles annealed at different annealing times: (a) 15 min, (b) 30 min, (c) 45 min and (d) 60 min.

where ( $\sigma_n$ ) is the electrical conductivity of ZnO film and ( $R_H$ ) is the Hall coefficient. It is clearly seen that the mobility increases with annealing time due to the grain growth; the dangling bonds at grain boundaries were reduced, while the carrier concentration decreased. The grain growth can be attributed to the coalescence of many grains after long time annealing. Figure 5 illustrates the schematic diagram of the ZnO/Si heterojunction and its room temperature  $I-V$  characteristics annealed at different times under no illumination in forward and reverse directions. All

heterojunctions exhibited good rectification characteristics, with the best value accomplished when the samples annealed for 45 min. The ideality factor ( $n$ ) of these heterojunctions was calculated from

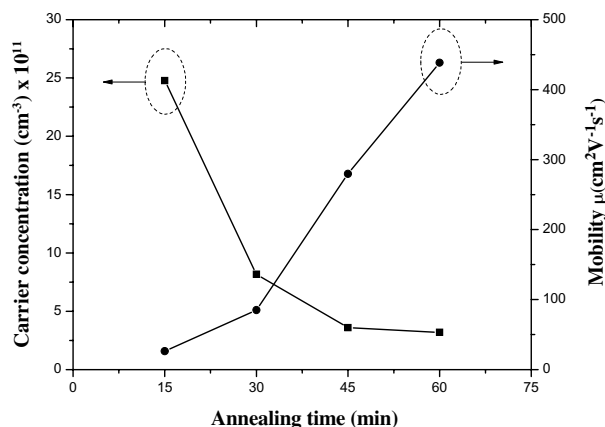


Fig. 4. Variation of mobility and carrier concentration of ZnO NPs films with annealing time.

Table 3. AFM data as function of annealing time.

$t_A$ (min)	RMS roughness (nm)	Average grain size (nm)
15	0.41	75.9
30	1.43	89.1
45	1.62	95.5
60	1.7	99.9

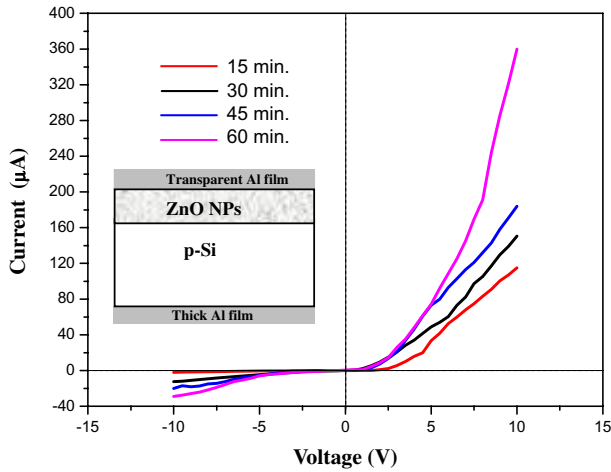


Fig. 5. Dark  $I$ - $V$  characteristics for ZnO/Si heterojunctions. Inset is the cross-sectional view of ZnO/Si heterojunction.

Table 4. Variation of ideality factor with annealing time.

Annealing time (min)	Ideality factor
15	5.3
30	4.5
45	4
60	3

semilogarithmic plots of  $I$ - $V$  characteristics and presented in Table 4 using the following relationship:

$$n = \frac{kT}{q} \frac{\Delta V}{Ln \frac{\Delta I}{I_s}}, \quad (2)$$

where  $k$  is Boltzman constant,  $T$  is the operating temperature and  $I_s$  is the saturation current. Large ideality factor values suggest the presence of recombination in the junction deposition and/or at junction interface<sup>27</sup> as well as some structural defects and large lattice mismatch between ZnO and silicon. The ideality factor has decreased after annealing due to the decreasing surface states and defects recombination at the interface. The current varied with bias voltage in different bias regions, indicating different mechanisms governing its value.<sup>28</sup> Soft breakdown was observed at bias voltage greater than 5 V. Figure 6 shows a linear relationship (abrupt junction) between  $(C^{-2}-V)$  at room temperature for ZnO/p-Si heterojunctions annealed at different times. The inset of Fig. 6 is the  $C$ - $V$  characteristic plot and the

built-in potential of all ZnO/p-Si is estimated by extrapolating the linear part of  $(C^{-2}-V)$  plot to the voltage axis. This was found to increase by increasing the annealing times. The turn-on voltage of the forward currents is larger than the built-in-potential due to the high series resistance and structural defects. The  $I$ - $V$  characteristics of illuminated heterojunction under different white light intensities are depicted in Fig. 7. All photodetectors exhibited good linearity characteristics with no significant saturation at high intensities. Maximum photo — to dark current ratio ( $I_{ph}/I_d$ ) was noticed for ZnO/Si heterojunction annealed at 60 min due to the decreasing recombination centers and structural defects. The visible light incident on ZnO/Si heterojunction passes through ZnO layer, get absorbed by silicon substrate and then e-h pairs are generated near the ZnO-Si interface.<sup>27</sup> Figure 8 demonstrates the spectral responsivity ( $R_\lambda$ ) plots of the ZnO/p-Si structure prepared at different annealing times for the wavelength range (350–900) nm at 7.5 V reverse bias. There are two peaks of response located at 650 nm and 870 nm with maximum responsivity of 0.39 A/W at 875 nm for the photodetector annealed for 60 min. The first peak is due to the absorption edge of ZnO film while, the second one is ascribed to the absorption edge of bulk silicon.<sup>29,30</sup> Longer annealing time improved the photodetectors responsivity and decreased both the structural defects and the recombination centers. The values of the obtained responsivity are comparable with that of ZnO/Si heterojunction prepared by spray pyrolysis. No shift in peak resonance was noticed at long annealing times. Results of detectivity  $D^*$  for annealed photodetectors are illustrated in Fig. 9. The detectivity was calculated using the following relationship:

$$D^* = \frac{R_\lambda (A \Delta f)^{0.5}}{I_n}, \quad (3)$$

where  $A$  is photosensitive area of photodetector,  $\Delta f$  is the bandwidth and  $I_n$  is the noise current. A detectivity of  $8 \times 10^{11} \text{ cm} \cdot \text{Hz}^{1/2} \text{W}^{-1}$  was obtained at 850 nm for n-ZnO/p-Si photodetector annealed at 60 min. This value is higher than that of other types of silicon-based heterojunction photodetector.<sup>31</sup> This high detectivity may indicate a reduced noise current after annealing for longer time due to decreased structural defects originated from trapping and recombination centers. The high detectivity could have

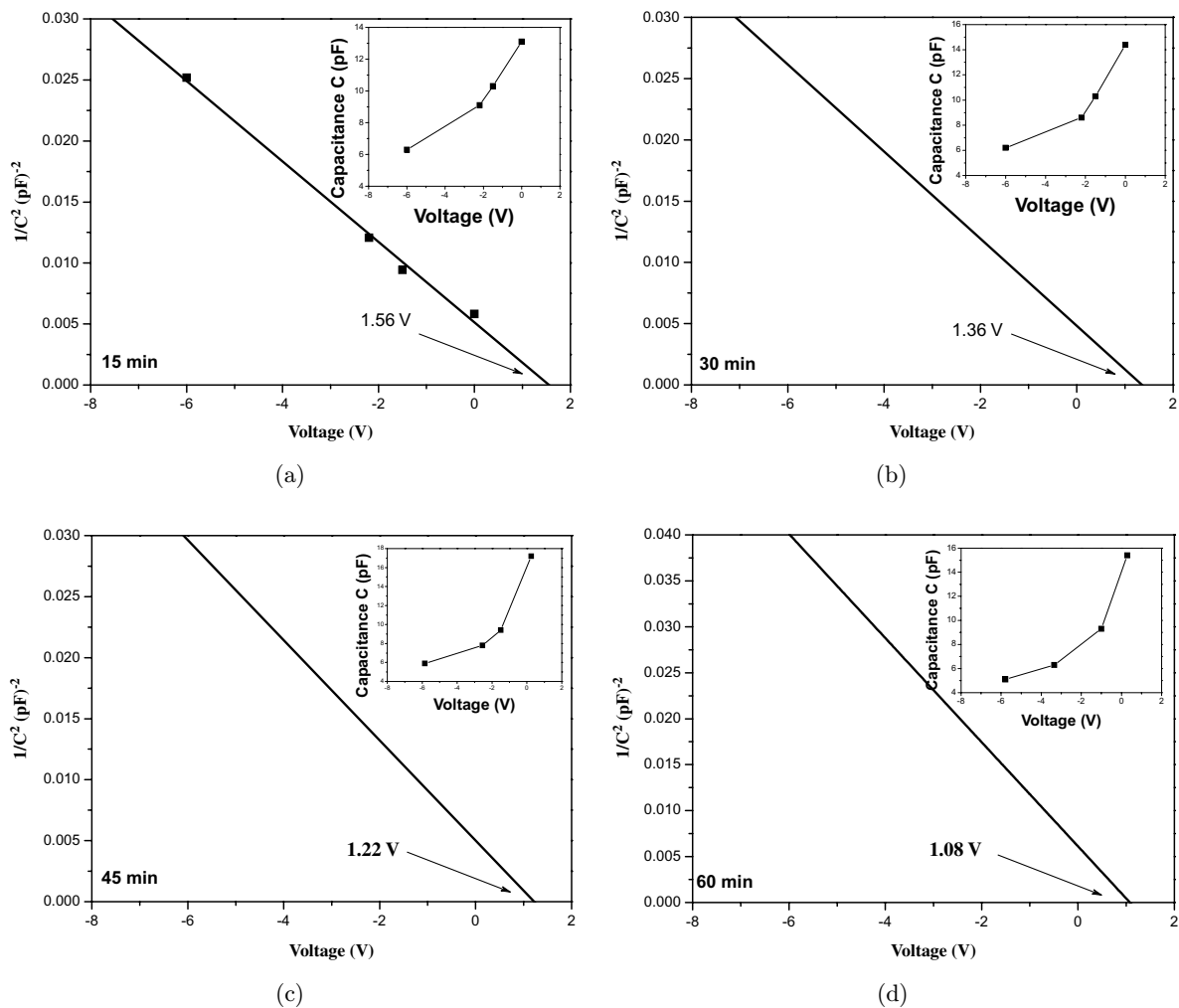


Fig. 6.  $1/C^{-2}-V$  plots for ZnO/Si heterojunction prepared at different annealing times: (a) 15 min (b) 30 min, (c) 45 min and (d) 60 min. Inset is a variation of junction capacitance with reverse bias voltage.

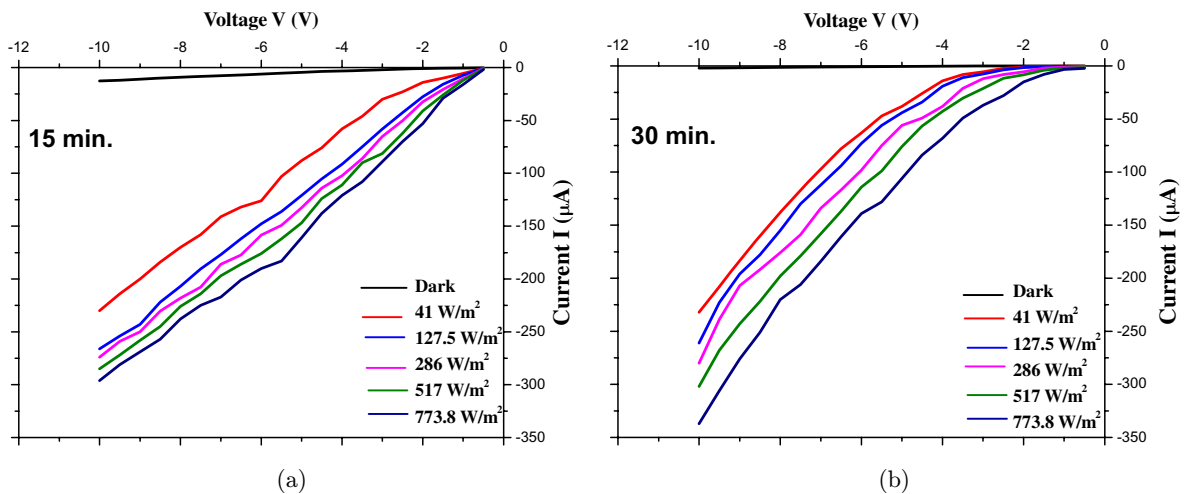


Fig. 7. Dark and illuminated  $I-V$  characteristics of ZnO/Si heterojunctions.

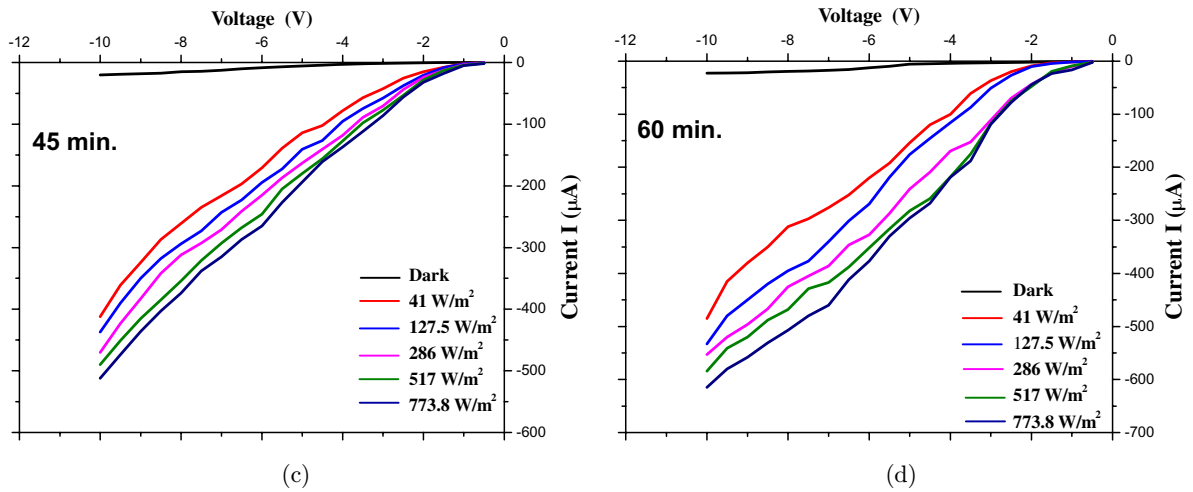


Fig. 7. (Continued)

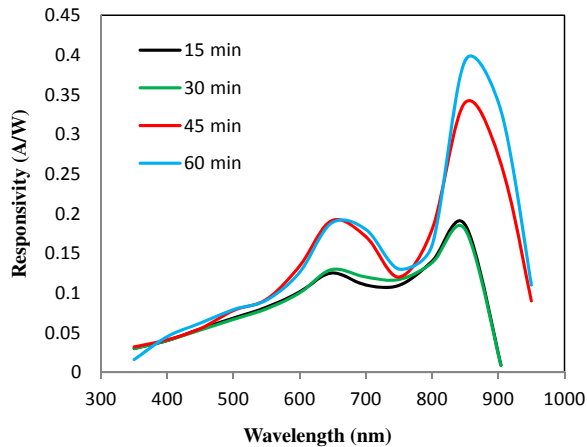


Fig. 8. Effect of annealing time on the spectral responsivity of ZnO/Si heterojunctions.

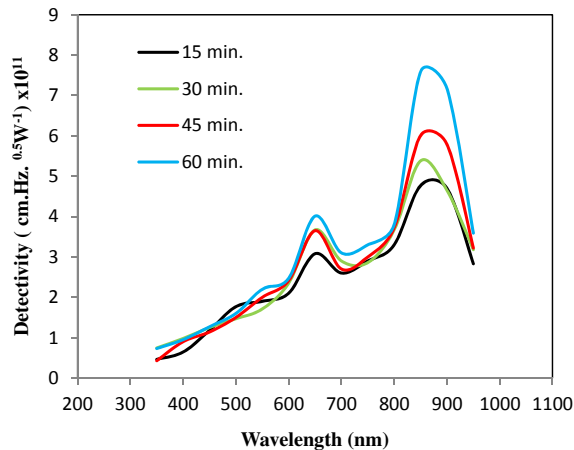
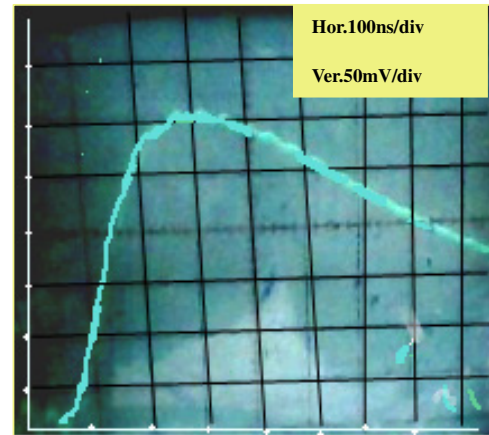
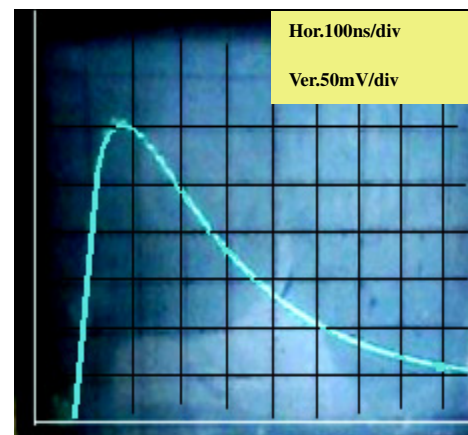


Fig. 9. Detectivity versus wavelength plot of ZnO/Si heterojunctions annealed at different annealing times.



(a)



(b)

Fig. 10. Laser pulse shape recorded by ZnO/Si photo-detectors (biased to  $-0.5$  V) annealed with different times: (a) 30 min and (b) 60 min.

Table 5. Rise time of photodetectors annealed at various times.

$t_A$ (min)	Rise time (ns)
15	180
30	150
45	100
60	50

otherwise resulted from increasing responsivity as shown in Fig. 8. Figure 10 shows some laser pulses recorded by photodetectors annealed at 45 and 60 min, indicating a 50 ns rise time for photodetector annealed at 60 min. Table 5 lists the effect of annealing time on the rise time of photodetectors. The long decay time indicates a response time not completely dominated by the RC product.

#### 4. Conclusions

High performance nanostructured ZnO/P-Si heterojunction photodetectors have been successfully fabricated using very simple and cost effective technique. The effect of annealing time on optical, structural and electrical properties of ZnO NPs was investigated. Figure of merit of these photodetectors was the annealing time dependent; with best photodetectors characteristics obtained after 60 min annealing. The  $C-V$  measurements suggested the formation of abrupt ZnO/p-Si heterojunction with annealing time dependent  $V_{bi}$  values. The high values of responsivity (0.39 A/W at 850 nm and 0.19 A/W at 650 nm) and detectivity ( $8.5 \times 10^{11} \text{ cm} \cdot \text{Hz}^{1/2} \text{ W}^{-1}$ ) may indicate a promising fabrication technique for inexpensive visible and near infra-red photodetectors.

#### References

1. T. P. Rao, M. C. Santhosh Kumar and V. Ganesan Indian, *J. Phys.* **85** (2011) 1381.
2. R. K. Sendi and S. Mahmud Indian, *J. Phys* **87** (2013) 523.
3. S. Chakraborty and P. Kumbhakar Indian, *J. Phys.* **88** (2014) 251.
4. Z. L. Wang, *J. Phys. Condens. Matter.* **16** (2004) R829.
5. Z. Fan and J. G. Lu, *J. Nanosci. Nanotechnol.* **5** (2005) 1561.
6. S. Baruah and J. Dutta, *Sci. Technol. Adv. Mater.* **10** (2009) 013001.
7. D. Wu, Z. Bai and K. Jiang, *Mater. Lett.* **63** (2009) 1057.
8. Z. Chen, Z. Shan, S. Li, C. B. Liang and S. X. Mao, *J. Cryst. Growth* **265** (2004) 482.
9. A. Sekar, S. H. Kim, A. Umar and Y. B. Hahn, *J. Cryst. Growth* **27** (2005) 7471.
10. B. P. Zhang, N. T. Binh, Y. Segawa, Y. Kashiwaba and K. Haga, *Appl. Phys. Lett.* **84** (2004) 586.
11. Y. C. Kong, D. P. Yu, B. Zhang, W. Fang and S. Q. Feng, *Appl. Phys. Lett.* **78** (2001) 407.
12. Y. J. Xing, Z. H. Xi, Z. Q. Xue, X. D. Zhang, J. H. Song, R. M. Wang, J. Xu, Y. Song, S. L. Zhang and D. P. Yu, *Appl. Phys. Lett.* **83** (2003) 1689.
13. W. I. Park, G.-C. Yi, M. Y. Kim and S. J. Pennycook, *Adv. Mater.* **15** (2003) 526.
14. L. Guo, S. Yang, C. Yang, P. Yu, J. Wang, W. Ge and G. K. L. Wong, *Appl. Phys. Lett.* **76** (2000) 2901.
15. Y. Wu, A. Tok, F. Boey, X. Zeng and X. Zhang, *Appl. Surf. Sci.* **253** (2007) 5473.
16. K. Haga, F. Katahira and H. Watanabe, *Thin Solid Films* **343** (1999) 145.
17. F. Zahedi and R. S. Dariani, *Thin Solid Films* **520** (2012) 2132.
18. S. A. Studenikin, N. Golego and M. Cocivera, *J. Appl. Phys.* **84** (1998) 2287.
19. W. Li, D. S. Mao, Z. H. Zheng, X. Wang, X. H. Liu, S. C. Zhu, Q. Li and J. F. Xu, *Surf. Coat. Technol.* **128** – **129** (2000) 346.
20. Y. Sun, G. M. Fuge and M. N. R. Ashfold, *Chem. Phys. Lett.* **396** (2004) 21.
21. W. Chiou, W. Wu and J. Ting, *Diam. Relat. Mater.* **12** (2003) 1841.
22. Y. Li, G. W. Meng, L. D. Zhang and F. Phillip, *Appl. Phys. Lett.* **7, 6** (2000) 2011.
23. S. Y. Li, C. Y. Lee and T. Y. Tseng, *J. Cryst. Growth* **247** (2003) 357.
24. X. Wang, Z. Cheng, K. Xu, H. Tsang and J.-B. Xu, *Nature Photon.* **7** (2013) 888.
25. J. Miao, W. Hu, N. Guo, Z. Lu, X. Liu, L. Liao, P. Chen, T. Jiang, S. Wu, J. Ho, L. Wan, X. Chen and W. Lu, doi: 10.1002/sml.201402312 (2015).
26. F. Yakuphanoglu, S. Ilican, M. Caglar and Y. Caglar, *J. Optoelectron Adv. Mater.* **9** (2007) 2180.
27. R. A. Ismail, K. Z. Yahya and O. A. Abdulrazaq, *Surf. Rev. Lett.* **12** (2005) 299.
28. T. Yun, W. Yan-Hua, Y. Wei, G. Wei and F. Guang-Sheng, *Chin. Phys. B* **21** (2012) 097105.
29. R. A. Ismail, A. Al-Naimi and A. A. Al-Ani, *Semicond. Sci. Technol.* **23** (2008) 075030.
30. R. A. Ismail, S. M. H. Al-Jawad and N. Hussein, *Appl. Phys. A* **117** (1977) 2014.
31. R. A. Ismail, *J. Semicond. Tech. Sci.* **6** (2006) 119.